

Gate-dependent spin-orbit coupling in multi-electron carbon nanotubes

T. S. Jespersen^{†,1} K. Grove-Rasmussen^{†,1,2} J. Paaske,¹ K. Muraki,² T. Fujisawa,³ J. Nygård,¹ and K. Flensberg¹

¹*Niels Bohr Institute & Nano-Science Center, University of Copenhagen,
Universitetsparken 5, DK-2100 Copenhagen, Denmark*

²*NTT Basic Research Laboratories, NTT Corporation,
3-1 Morinosato-Wakamiya, Atsugi 243-0198, Japan*

³*Research Center for Low Temperature Physics, Tokyo Institute of Technology, Ookayama, Meguro, Tokyo 152-8551, Japan*

Understanding how the orbital motion of electrons is coupled to the spin degree of freedom in nanoscale systems is central for applications in spin-based electronics and quantum computation. We demonstrate this coupling of spin and orbit in a carbon nanotube quantum dot in the general multi-electron regime in presence of finite disorder. Further, we find a strong systematic dependence of the spin-orbit coupling on the electron occupation of the quantum dot. This dependence, which even includes a sign change is not demonstrated in any other system and follows from the curvature-induced spin-orbit split Dirac-spectrum of the underlying graphene lattice. Our findings unambiguously show that the spin-orbit coupling is a general property of nanotube quantum dots which provide a unique platform for the study of spin-orbit effects and their applications.

Note: Manuscript with high resolution figures and supplement at

www.fys.ku.dk/~tsand/TSJ_KGR2010.pdf

The interaction of the spin of electrons with their orbital motion has become a focus of attention in quantum dot research. On the one hand, this spin-orbit interaction (SOI) provides a route for spin decoherence, which is unwanted for purposes of quantum computation[1–3]. On the other hand, if properly controlled, the SOI can be utilized as a means of electrically manipulating the spin degree of freedom[4–7].

In this context, carbon nanotubes provide a number of attractive features, including large confinement energies, nearly nuclear-spin-free environment, and, most importantly, the details of the energy level structure is theoretically well understood and modeled, as well as experimentally highly reproducible. Remarkably, the SOI in nanotubes was largely overlooked in the first two decades of nanotube research and was only recently demonstrated by Kuemmeth *et al.* for the special case of a single carrier in ultra-clean CNT quantum dots[2, 8, 9]. Except for these reports, the SOI in nanotubes is experimentally unexplored. Theoretically, the focus has exclusively been on the SOI-modified band structure of disorder-free nanotubes[10–14]. Therefore, two important questions remain: how the effective SOI depends on electron filling and how it appears in the general case of quantum dots subject to disorder. Here we answer these two questions.

Firstly, by low-temperature electron transport we demonstrate the presence of a significant SOI in a disordered CNT quantum dot holding hundreds of electrons. We identify and analyze the role of SOI in the energy spectrum for one, two, and three electrons in the four-fold degenerate CNT electronic shells, thus describing shells at any electron filling. By rotating the sample, we present for the first time spectroscopy of the same charge-states for magnetic fields both parallel and perpendicular to the nanotube axis, thus controlling the coupling to the orbital magnetic moment. Remarkably,

a single-electron model taking into account both SOI and disorder quantitatively describes all essential details of the multi-electron quantum dot spectra. Secondly, by changing the electron occupancy we are able to tune the effective SOI and even reverse its sign in accordance with the expected curvature-induced spin-orbit splitting of the underlying graphene Dirac spectrum[1, 11–14]. Such systematic dependence has not been demonstrated in any other material system and may enable a new range of spin-orbit related applications. This microscopic understanding and detailed modeling is in stark contrasts to situations encountered in alternative strong-SOI quantum-dot materials, such as InAs or InSb nanowires, where the effective SOI arises from bulk crystal effects combined with unknown contributions from surface effects, strain and crystal defects[15]. These systems often exhibit semi-random fluctuations of, e.g., the g -factor as single electrons are added[16, 17]. Thus, beyond fundamental interest and the prospect of realizing recent proposals of SOI-induced spin control in CNTs[1, 18], our findings pave the way for new designs of experiments utilizing the SOI in quantum dots.

Zero-field splitting of the four-fold degeneracy

Our experimental setup is presented in Fig. 1a. We fabricate devices of single-wall CNTs on highly doped Si substrates capped with an insulating layer of SiO₂ (see Methods section). The size of the quantum dots is defined by the contact separation (400 nm) and the electrical properties are investigated in a voltage biased two-terminal configuration applying a voltage V_{sd} between source-drain contacts and measuring the resulting current I . The differential conductance dI/dV_{sd} is measured by standard lock-in techniques. When biased with a voltage V_g , the Si substrate acts as an electrostatic gate controlling the electron occupancy of the dot. The devices are measured at $T = 100$ mK in a ³He/⁴He

dilution refrigerator, fitted with a piezo-rotator allowing in-plane rotations of the device in magnetic fields up to 9 T.

Figure 1b shows a typical measurement of dI/dV_{sd} vs. V_{sd} and V_g in the multi-electron regime of a small-band-gap semiconducting nanotube. The pattern of diamond-shaped regions of low conductance is expected for a quantum dot in the Coulomb blockade regime and within each diamond the quantum dot hosts a fixed number of electrons N , increasing one-by-one with increasing V_g . The energy E_{add} , required for adding a single electron appears as the diamond heights and has been extracted in Fig. 1c. The four-electron periodicity clearly observed in Fig. 1b and c reflects the near four-fold degeneracy in the nanotube energy spectrum[19, 20]; one factor of 2 from the intrinsic spin (\uparrow, \downarrow) and one factor of 2 from the so-called isospin (K, K') that stems from the rotational symmetry of the nanotube - electrons orbit the CNT in a clockwise or anticlockwise direction. As is generally observed[19–23], the addition energy for the second electron in each quartet (yellow in Fig. 1c) exceeds those for one and three. This was previously interpreted as a result of disorder-induced coupling $\Delta_{KK'}$ of the clockwise and anticlockwise states[21, 24] that splits the spectrum into two spin-degenerate pairs of bonding/antibonding states separated by $\Delta_{KK'}$. As mentioned, Kuemmeth *et al.* showed recently that for the first electron in an ultra-clean suspended nanotube quantum dot, the splitting was instead dominated by the spin-orbit coupling. The first question we address here is whether SOI also appears in the many-electron regime and how it may be modified or masked by disorder.

Modeling spin-orbit coupling and disorder

Performing level spectroscopy with a magnetic field B applied either parallel (B_{\parallel}) or perpendicular (B_{\perp}) to the nanotube axis proves to be a powerful tool to analyze the separate contributions from disorder and spin-orbit coupling. This is illustrated in Figs. 2a-d, which show calculated single-particle energy level spectra for four limiting combinations of $\Delta_{KK'}$ and the effective spin-orbit coupling Δ_{SO} (all limits are relevant for nanotube devices depending on the degree of disorder and CNT structure[13, 14]; details of the model are provided in the Supplementary Information). In all cases a parallel field separates the four states into pairs of increasing (K -like states) and decreasing (K' -like states) energies. The magnitude of the shift is given by the orbital g -factor g_{orb} reflecting the coupling of B_{\parallel} to the orbital magnetic moment caused by motion around the CNT[25]. Further, each pair exhibits a smaller internal splitting due to the Zeeman effect. Figure 2b shows the disorder induced coupling of K and K' states resulting in an avoided crossing at $B_{\parallel} = 0$ and the zero-field splitting discussed above. In the opposite limit with SOI only (Fig. 2c), the

zero-field spectrum is also split into two doublets, but the field dependence is markedly different and no avoided crossing appears. In the simplest picture, this behavior originates from coupling of the electron spin to an effective magnetic field $\mathbf{B}_{SO} = -(\mathbf{v} \times \mathbf{E})/c^2$ experienced by the electron as it moves with velocity \mathbf{v} in an electric field \mathbf{E} . Here the speed of light, c , reflects the relativistic origin of the effect. In nanotubes, the curvature of the graphene lattice generates an effective radial electric field, and since the velocity is mainly circumferential (and opposite for K and K'), \mathbf{B}_{SO} polarizes the spins along the nanotube axis and favors parallel alignment of the spin and orbital angular momentum. Thus, even in the absence of disorder, the spectrum splits into two Kramers doublets ($K \downarrow, K' \uparrow$) and ($K \uparrow, K' \downarrow$) separated by Δ_{SO} . Interestingly, since a perpendicular field does not couple K and K' the doublets do not split along B_{\perp} on the figure. As a consequence, the g -factor, when measured in a perpendicular field, will vary from *zero* when $\Delta_{SO} \gg \Delta_{KK'}$ (Fig. 2c) to 2 in the opposite limit (Fig. 2b).

The final case, including both disorder and SOI, is of particular importance for the present study, and the calculated spectrum is displayed in Fig. 2d for $\Delta_{KK'} > \Delta_{SO}$. Importantly, the effects of SOI are not masked despite the dominating disorder: For parallel field, SOI remains responsible for an asymmetric splitting of the Kramers doublets (α, β) vs. (δ, γ), and the appearance of an additional degeneracy in the spectrum at finite field (δ and γ states). In a perpendicular field, the effect of SOI is to suppress the Zeeman splitting of the two doublets and since the eigenstates of the SOI have spins along the nanotube axis it couples the states with spins polarized along B_{\perp} resulting in the avoided crossing indicated on the figure.

Spin-orbit interaction revealed by spectroscopy

With this in mind we now focus on the quartet with $4N_0 \approx 180$ electrons highlighted in Fig. 1b and expanded in Fig. 3a. In order to investigate the level structure we perform cotunneling spectroscopy, as illustrated in the schematic Fig. 3b[26]: In Coulomb blockade, whenever $e|V_{sd}|$ matches the energy of a transition from the ground state α to an excited state (β, γ, δ), inelastic cotunnel processes, that leave the quantum dot in the excited state, become available for transport. This significantly increases the current and gives rise to steps in the conductance. These appear as gate-independent features in Fig. 3a (arrows) and are clearly seen in the inset showing a trace through the center of the one-electron ($4N_0 + 1$) diamond along the dashed line. Thus following the magnetic field dependence of this trace, as shown in Fig. 3c, maps out the level structure. The energies of the excitations are given by the inflection points of the curve (*i.e.* peaks/dips of d^2I/dV_{sd}^2)[27] and the level

evolution is therefore directly evident in Fig. 3d-i, which show color maps of the second derivative vs. V_{sd} and B_{\perp}, B_{\parallel} for V_g positioned in the center of the one, two, and three electron charge states. As explained below, the SOI is clearly expressed in all three spectra.

Consider first the one-electron case: In a parallel field (Fig. 3d), the asymmetric splitting of the two doublets is evident (black vs. green arrows) and applying the field perpendicularly (Panel g), the SOI is directly expressed as the avoided crossing indicated on the figure. The measurement is in near-perfect agreement with the single-particle excitation spectrum calculated by subtracting the energies of Fig. 3b and shown by the solid lines. The calculation depends on only three parameters: $\Delta_{SO} = 0.15$ meV set directly by the avoided crossing, $\Delta_{KK'} = 0.45$ meV determined from the zero-field splitting of the doublets (see Fig. 2d), and $g_{orb} = 5.7$ set by the slopes of the excitation lines from α to γ, δ in Panel d.

Consider now the role of SOI for the doubly occupied CNT quartet. This situation is of particular importance for quantum computation as a paradigm for preparation of entangled states and a fundamental part of Pauli blockade in double quantum dots[28]. Figures 3e,h show the measured spectra in parallel and perpendicular fields. The model perfectly describes the measurement and now contains no free parameters since these are fixed by one-electron measurement. Six states are expected: the ground state singlet-like state \tilde{S}_0 formed by the two electrons occupying the low-energy Kramers doublet[29], three triplet-like $\tilde{T}_-, \tilde{T}_0, \tilde{T}_+$ and a singlet-like state \tilde{S}_1 , which all use one state from each doublet and the singlet-like \tilde{S}_2 with both electrons occupying the high-energy doublet. The ground state \tilde{S}_0 does not appear directly in the measurement, but sets the origin for the cotunneling excitations. The excitation to the high-energy \tilde{S}_2 (dashed line) is absent in the experiment, since it cannot be reached by promoting only a single electron from \tilde{S}_0 . In Fig. 3h excitations to \tilde{T}_- and \tilde{T}_+ are clearly observed, while \tilde{S}_1 and \tilde{T}_0 merge into a single high-intensity peak showing that any exchange splitting J is below the spectroscopic line width $\approx 100\mu\text{eV}$ [23]. In other quartets an exchange splitting is indeed observed (see Supplementary Information). In the two-electron spectra the SOI is directly expressed as the avoided crossing at $B_{\perp} \approx 4.5$ T accompanying the $\tilde{S}_0 \leftrightarrow \tilde{T}_-$ ground state transition[15, 30]. In quartets of yet stronger tunnel-coupling it is replaced by a singlet-triplet Kondo resonance[31] (see Supplementary Information).

Finally, the spectrum of three electrons in the four-electron shell is equivalent to that of a single hole in a full shell; at low fields the δ -state becomes the ground-state and γ the first excited state, while α and β then constitute the excited doublet. As seen by comparing Fig. 2b and 2d SOI breaks the intra-shell electron-hole symmetry of the nanotube spectrum. This is evident in the experiment when comparing Fig. 3d

and 3f: In 3f, increasing B_{\parallel} , the lowest excited state γ , barely separates from the ground state δ and at $B_{\parallel} = 1.1$ T they cross again, causing a ground state transition. At the crossing point, the spin-degenerate ground-state results in a zero-bias Kondo peak (see inset)[32]. Interestingly, this degeneracy also forms the qubit proposed in Ref. 1. For the B_{\perp} -dependence the one- and three-electron cases remain identical and Fig. 3i exhibits again the SOI-induced avoided crossings.

Gate-dependent spin-orbit coupling

Having established the presence of SOI in the general many-electron disordered quantum dot, we now focus on the dependence of Δ_{SO} on the quantum dot occupation. To this end, we have repeated the spectroscopy of Fig. 3 for a large number of CNT quartets and in each case extracted Δ_{SO} by fitting to the single-particle model (all underlying data are presented in the Supplementary Information). Figure 4a shows the result as a function of V_g . An overall decrease of Δ_{SO} is observed as electrons are added to the conduction band and, interestingly, a negative value is found in the valence band (*i.e.* SOI favoring anti-parallel rather than parallel spin and orbital angular momentum, thus effectively interchanging the one and three-electron spectra).

The magnitude of Δ_{SO} is given by the spin-orbit splitting of the underlying graphene band structure as we will now discuss. For flat graphene this splitting is very weak ($\Delta_{SO}^{graphene} \sim 1\mu\text{eV}$)[12] as it is second-order in the already weak atomic SOI of carbon $\Delta_{SO}^C \sim 8$ meV. In nanotubes, however, the curvature induces a coupling between the π - and σ -bands and generates a curvature-induced spin-orbit splitting, which is first order in the atomic SOI and thus greatly enhances Δ_{SO} . Around a Dirac-point of the Brillouin zone (*e.g.* K) the graphene band structure appears as on Fig. 4b[11–14]: The spin-up and spin-down Dirac cones are split by SOI both in energy and along k_{\perp} , the momentum in the circumferential direction of the CNT. The schematic also highlights the CNT band structure (Fig. 4a upper inset) obtained by imposing periodic boundary conditions on k_{\perp} . In a finite-length CNT quantum dot also the wavevector along the nanotube axis, k_{\parallel} , is quantized, and letting ϵ_N denote the energy of the N^{th} longitudinal mode the effective SOI for a small-gap CNT becomes

$$\begin{aligned} \Delta_{SO,\pm} &= E_{\uparrow}^K - E_{\downarrow}^K \\ &= 2\Delta_{SO}^0 \pm \sqrt{(\Delta_g + \Delta_{SO}^1)^2 + \epsilon_N^2} \\ &\mp \sqrt{(\Delta_g - \Delta_{SO}^1)^2 + \epsilon_N^2}. \end{aligned} \quad (1)$$

Here the upper(lower) sign refers to the conduction(valence) band, Δ_g is the curvature induced energy gap[33, 34], and the two terms Δ_{SO}^0 and Δ_{SO}^1 are the band structure spin-orbit parameters due to

curvature[11–14]. The separate contributions of the two terms are illustrated in the lower inset to Fig. 4a. Δ_{SO}^1 was found already in the work of Ando[10] and accounts for the k_{\perp} -separation of the Dirac-cones in Fig. 4b. For the CNT band structure this term acts equivalently to an Aharonov-Bohm flux from a parallel spin-dependent magnetic field, which changes the quantization conditions in the k_{\perp} -direction. Characteristically, its contribution to Δ_{SO} decreases with the number of electrons in the dot (ϵ_N) and reverses sign for the valence band. This contrasts the ϵ_N -independent contribution from the recently predicted Δ_{SO}^0 -term[12–14], which acts as an effective valley-dependent Zeeman term and accounts for the energy splitting of the Dirac-cones in Fig. 4b. For the nanotube studied in Kuemmeth *et al.* [9] Δ_{SO} has the same sign for electrons and holes, *i.e.*, $|\Delta_{SO}^0| > |\Delta_{SO}^1|$. In our case, the negative values measured in the valence band demonstrate the opposite limit $|\Delta_{SO}^0| < |\Delta_{SO}^1|$. Thus, the measured gate-dependence of Δ_{SO} agrees with the spin-orbit splitting of the graphene Dirac spectrum caused by the curvature of the nanotube, and fitting to Eq. 1 (Fig. 4a, dashed line) yields $\Delta_{SO}^0 = 10 \pm 10 \mu\text{eV}$ and $\Delta_{SO}^1 = 220 \pm 25 \mu\text{eV}$ [35]. Band structure models relate these parameters to the structure of the nanotube[12–14]: $\Delta_{SO}^0 = \lambda_0 \Delta_{SO}^C \Delta_g D$ and $\Delta_{SO}^1 = \lambda_1 \Delta_{SO}^C / D$, where D is the nanotube diameter and $\lambda_{1,2}$ constants that depend on the CNT class (semiconducting, small-band-gap). Typically CVD-grown single wall CNTs have diameters in the range 1-3 nm, while obtaining D from the measured values of g_{orb} [36] gives $D \approx 6$ nm. Thus taking $D = 1-6$ nm we estimate $\lambda_1 = 0.03-0.17$ nm and $\lambda_0 = 0.7-4 \cdot 10^{-6} (\text{nm} \cdot \text{meV})^{-1}$. While λ_1 is consistent with the value quoted in the theoretical literature (0.095 nm)[13], the calculated λ_0 value $-4 \cdot 10^{-3} (\text{nm} \cdot \text{meV})^{-1}$ does not match the experiment and similar deviations appear[13] when comparing the theory to the SOI values measured in Ref. 8. The origin of this discrepancy remains unknown, and further work on SOI in nanotubes with known chirality is needed to make further progress.

Methods

The devices are made on a highly doped Silicon wafer terminated by 500 nm of SiO_2 . Alignment marks (Cr, 70 nm) are defined by electron beam lithography prior to deposition of catalyst islands made of Iron nitrate ($\text{Fe}(\text{NO}_3)_3$), Molybdenum acetate and Alumina support particles[37]. The sample is then transferred to a furnace, where single wall carbon nanotubes are grown by chemical vapor deposition at 850-900°C in an atmosphere of hydrogen, argon and methane gases. Pairs of electrodes consisting of Au/Pd (40/10 nm) spaced by 400 nm are fabricated alongside the catalyst islands by standard electron beam lithography techniques. Finally, bonding pads (Au/Cr 150/10 nm) are made by optical lithography and the devices are screened by room- and low-temperature measurements.

We measured the sample in an Oxford dilution refrigerator fitted with an Attocube ANRv51 piezo rotator which allows high precision in-plane rotation of the sample in large magnetic fields. The rotator provides resistive feedback of the actual position measured by lock-in techniques. For electrical filtering, room-temperature π -filters and low-temperature Thermocoax are used. The base temperature of the modified refrigerator is around 100 mK. The CNT measurement setup consists of a National Instrument digital to analog card, custom made optically coupled amplifiers, a DL Instruments 1211 current to voltage amplifier and a Princeton Applied Research 5210 Lock-in amplifier. Standard dc and lock-in techniques have been used to measure current and differential conductance dI/dV_{sd} while d^2I/dV_{sd}^2 is obtained numerically.

- [1] Bulaev, D., Trauzettel, B. & Loss, D. Spin-orbit interaction and anomalous spin relaxation in carbon nanotube quantum dots. *Phys. Rev. B* **77**, 235301 (2008).
- [2] Churchill, H. *et al.* Electron-nuclear interaction in c-13 nanotube double quantum dots. *Nat. Phys.* **5**, 321 – 326 (2009).
- [3] Fischer, J. & Loss, D. Dealing with decoherence. *Science* **324**, 1277–1278 (2009).
- [4] Flindt, C., Sørensen, A. & Flensberg, K. Spin-orbit mediated control of spin qubits. *Phys. Rev. Lett.* **97**, 240501 (2006).
- [5] Nowack, K., Koppens, F., Nazarov, Y. & Vandersypen, L. Coherent control of a single electron spin with electric fields. *Science* **318**, 1430 – 1433 (2007).
- [6] Pfund, A., Shorubalko, I., Ensslin, K. & Leturcq, R. Suppression of spin relaxation in an inas nanowire double quantum dot. *Phys. Rev. Lett.* **99**, 036801 (2007).
- [7] Trif, M., Golovach, V. & Loss, D. Spin-spin coupling in electrostatically coupled quantum dots. *Phys. Rev. B* **75**, 085307 (2007).
- [8] Kuemmeth, F., Churchill, H., Herring, P. & Marcus, C. Carbon nanotubes for coherent spintronics. *Mat. Today* **13**, 18–26 (2010).
- [9] Kuemmeth, F., Ilani, S., Ralph, D. & McEuen, P. Coupling of spin and orbital motion of electrons in carbon nanotubes. *Nature* **452**, 448 – 452 (2008).
- [10] Ando, T. Spin-orbit interaction in carbon nanotubes. *J. Phys. Soc. Jpn.* **69**, 1757 – 1763 (2000).
- [11] Chico, L., Lopez-Sancho, M. & Munoz, M. Spin splitting induced by spin-orbit interaction in chiral nanotubes. *Phys. Rev. Lett.* **93**, 176402 (2004).
- [12] Huertas-Hernando, D., Guinea, F. & Brataas, A. Spin-orbit coupling in curved graphene, fullerenes, nanotubes, and nanotube caps. *Phys. Rev. B* **74**, 155426 (2006).
- [13] Izumida, W., Sato, K. & Saito, R. Spin-orbit interaction in single wall carbon nanotubes: Symmetry adapted tight-binding calculation and effective model analysis. *J. Phys. Soc. Jpn.* **78**, 074707 (2009).
- [14] Jeong, J. & Lee, H. Curvature-enhanced spin-orbit coupling in a carbon nanotube. *Phys. Rev. B* **80**, 075409 (2009).
- [15] Fasth, C., Fuhrer, A., Samuelson, L., Golovach, V. & Loss, D. Direct measurement of the spin-orbit interaction in a two-electron inas nanowire quantum dot. *Phys. Rev. Lett.* **98**, 266801 (2007).
- [16] Csonka, S. *et al.* Giant fluctuations and gate control of the g -factor in inas nanowire quantum dots. *Nano Lett.* **8**, 3932–3935 (2008).
- [17] Nilsson, H. *et al.* Giant, level-dependent g factors in insb nanowire quantum dots. *Nano Lett.* **9**, 3151–3156 (2009).
- [18] Flensberg, K. & Marcus, C. Bends in nanotubes allow electric spin control and coupling. *Phys. Rev. B* **81**, 195418 (2010).
- [19] Cobden, D. & Nygard, J. Shell filling in closed single-wall carbon nanotube quantum dots. *Phys. Rev. Lett.* **89**, 046803 (2002).
- [20] Liang, W., Bockrath, M. & Park, H. Shell filling and exchange coupling in metallic single-walled carbon nanotubes. *Phys. Rev. Lett.* **88**, 126801 (2002).
- [21] Jarillo-Herrero, P. *et al.* Electronic transport spectroscopy of carbon nanotubes in a magnetic field. *Phys. Rev. Lett.* **94**, 156802 (2005).
- [22] Makarovski, A., An, L., Liu, J. & Finkelstein, G. Persistent orbital degeneracy in carbon nanotubes. *Phys. Rev. B* **74**, 155431 (2006).
- [23] Moriyama, S., Fuse, T., Suzuki, M., Aoyagi, Y. & Ishibashi, K. Four-electron shell structures and an interacting two-electron system in carbon-nanotube quantum dots. *Phys. Rev. Lett.* **94**, 186806 (2005).
- [24] Oreg, Y., Byczuk, K. & Halperin, B. Spin configurations of a carbon nanotube in a nonuniform external potential. *Phys. Rev. Lett.* **85**, 365–368 (2000).
- [25] Minot, E., Yaish, Y., Sazonova, V. & Mceuen, P. Determination of electron orbital magnetic moments in carbon nanotubes. *Nature* **428**, 536 – 539 (2004).
- [26] De Franceschi, S. *et al.* Electron cotunneling in a semiconductor quantum dot. *Phys. Rev. Lett.* **86**, 878–881 (2001).
- [27] Paaske, J. *et al.* Non-equilibrium singlet-triplet kondo effect in carbon nanotubes. *Nat. Phys.* **2**, 460–464 (2006).
- [28] Hanson, R., Kouwenhoven, L., Petta, J., Tarucha, S. & Vandersypen, L. Spins in few-electron quantum dots. *Rev. Mod. Phys.* **79**, 1217–1265 (2007).
- [29] The states are not the conventional spin singlets and triplets as they are modified by SOI as emphasized by the tildes.
- [30] From the high-field ground state \tilde{T}_- , excitations to \tilde{S}_2 are actually allowed, however, the $\tilde{S}_0 \leftrightarrow \tilde{T}_-$ and $\tilde{S}_2 \leftrightarrow \tilde{T}_+$ avoided crossings occur simultaneously and as \tilde{T}_- to \tilde{T}_+ excitations are forbidden the dashed line remains unseen in the experiment.
- [31] Nygard, J., Cobden, D. & Lindelof, P. Kondo physics in carbon nanotubes. *Nature* **408**, 342–346 (2000).
- [32] Galpin, M., Jayatilaka, F., Logan, D. & Anders, F. Interplay between kondo physics and spin-orbit coupling in carbon nanotube quantum dots. *Phys. Rev. B* **81**, 075437 (2010).
- [33] Kane, C. & Mele, E. Size, shape, and low energy electronic structure of carbon nanotubes. *Phys. Rev. Lett.* **78**, 1932–1935 (1997).
- [34] Kleiner, A. & Eggert, S. Band gaps of primary metallic carbon nanotubes. *Phys. Rev. B* **63**, 073408 (2001).
- [35] The band-gap of the device $E_g \approx 30$ meV is measured directly as a large Coulomb diamond at $V_g \approx 1$ V and $\epsilon_N \approx 25$ meV/V $\times V_g$ is estimated from the level spacing $\Delta E \approx 3$ meV and ≈ 8 shells/V.
- [36] Within the present theory the orbital g -factor depends on electron filling $g_{\text{orb}} \approx (e v_F D / 2 \mu_B) / \sqrt{1 + (\epsilon_n / \Delta_g)^2}$ in agreement with the measurements (see SOM).
- [37] Kong, J., Soh, H., Cassell, A., Quate, C. & Dai, H. Synthesis of individual single-walled carbon nanotubes on patterned silicon wafers. *Nature* **395**, 878–881 (1998).

Acknowledgements

We thank P. E. Lindelof, J. Mygind, H.I. Jørgensen, C.M. Marcus, and F. Kuemmeth for discussions and experimental support. T.S.J. acknowledges the Carlsberg Foundation and Lundbeck Foundation for financial sup-

port. K.G.R. K.F. J.N. acknowledges The Danish Research Council and University of Copenhagen Center of Excellence.

rotating sample stage. K.G.R. made the sample. K.M., T.F. and J.N. participated in discussions and writing the paper. J.P. and K.F. developed the theory and guided the experiment.

Author contributions

T.S.J. and K.G.R. performed the measurements, analyzed the data and wrote the paper. T.S.J. designed the

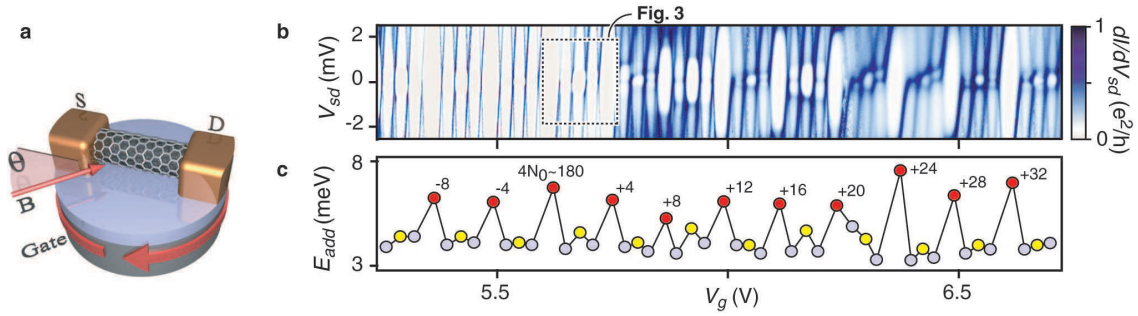


FIG. 1: Four-fold periodic nanotube spectrum. **a**, Schematic illustration of the device and setup. CNT quantum dots are measured at $T = 100$ mK in a standard two-terminal configuration in a cryostat modified to enable measurements in a high magnetic field at arbitrary in-plane angles θ to the CNT axis. **b**, Typical measurement of the differential conductance dI/dV_{sd} vs. source-drain bias V_{sd} and gate voltage V_g for a multi-electron CNT quantum dot. **c**, Addition energy as a function of V_g . In **b** and **c** the characteristic filling of four-electron shells is clearly seen.

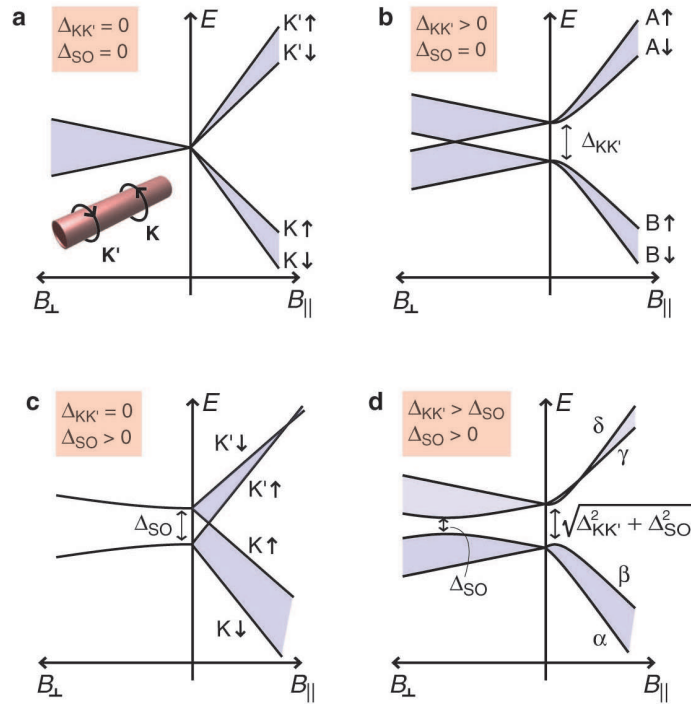


FIG. 2: Role of spin-orbit interaction and disorder for the nanotube energy spectrum. Calculated single-particle energy spectrum as a function of magnetic field applied perpendicular (B_{\perp}) and parallel (B_{\parallel}) to the CNT axis in the limiting cases of neither SOI nor disorder **a**, disorder alone **b**, SOI alone **c**, and the two combined $\Delta_{KK'} > \Delta_{SO} > 0$ **d**. Depending on the CNT type, electron filling and degree of disorder, all four situations can occur.

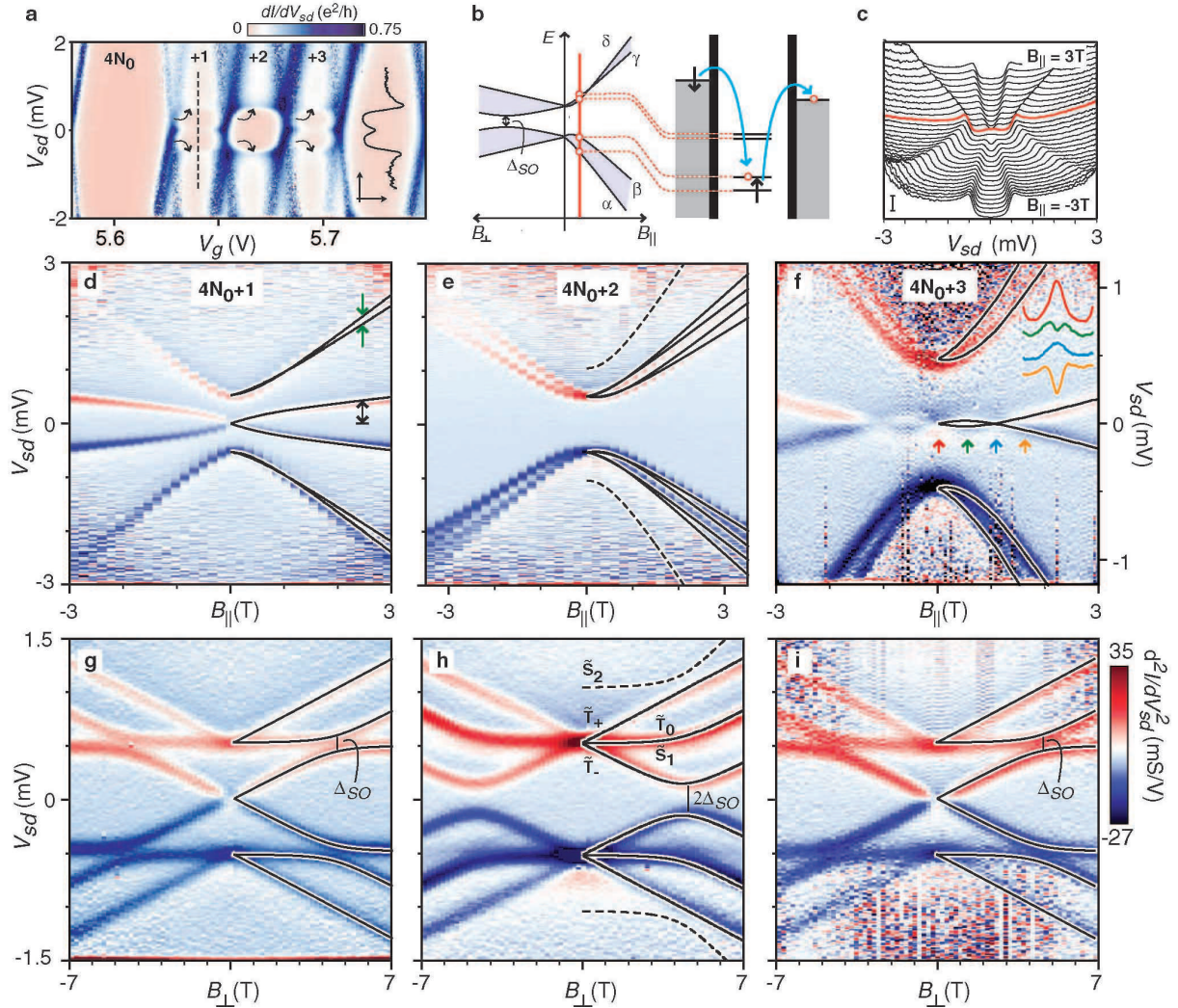


FIG. 3: Spin-orbit interaction in a disordered multi-electron nanotube quantum dot. **a**, Measurement of dI/dV_{sd} vs. V_{sd} and V_g corresponding to the consecutive addition of four electrons to an empty shell (indicated on Fig. 1b). A strong tunnel coupling results in significant cotunneling which is evident as horizontal lines truncating the diamonds (arrows). The black trace shows a cut along the dashed line. **b**, Schematic illustration of the relevant inelastic cotunneling processes. **c**, Traces along the dashed line in **a** for various $B_{||}$ (red: $B = 0$, scale-bar: $0.1e^2/h$). **d-f**, The *second derivative* d^2I/dV_{sd}^2 along the center of the $N_0 + 1$, $N_0 + 2$ and $N_0 + 3$ diamonds, respectively, as a function of a parallel magnetic field. Peaks/dips appear at inflection points of the differential conductance and thus correspond to the energy difference between ground and excited states. In **f** the inset shows dI/dV_{sd} vs. $-0.3 < V_{sd} < 0.3$ mV and $B_{||} = 0; 0.55; 1.1; 1.65$ T (arrows) illustrating the splitting and SOI-induced reappearance of a zero-bias Kondo resonance. **g-i**, As **d-f** but measured as a function of B_{\perp} . The effective spin-orbit coupling appears directly as the avoided crossings indicated by Δ_{SO} . In **d-i** the black lines results from the single-particle model with parameters $\Delta_{SO} = 0.15$ meV, $\Delta_{KK'} = 0.45$ meV, and $g_{orb} = 11.4$. The dashed lines in **e,h** correspond to the excitations to the two-electron singlet-like \tilde{S}_2 state which cannot be reached by promoting a single electron from the ground state (\tilde{S}_0) and therefore expected to be absent in the measurement.

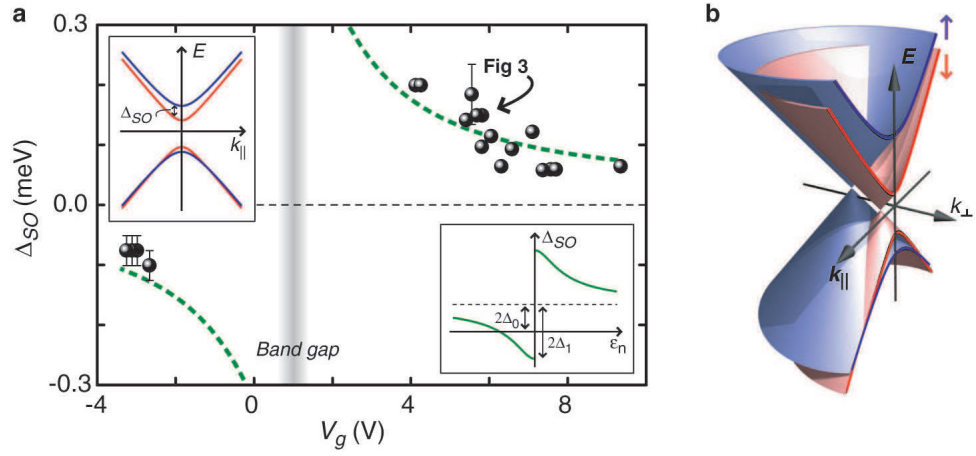


FIG. 4: Tuning Δ_{SO} in accordance with the curvature-induced spin-orbit splitting of the nanotube Dirac-spectrum. **a**, Measured effective spin-orbit coupling strength as a function of V_g extracted from spectroscopy measurements like in Fig. 3, repeated for multiple shells. The dashed line is a fit to the theory. Lower inset: Expected dependence of Δ_{SO} on ϵ_N highlighting the two SOI-contributions Δ_{SO}^0 and Δ_{SO}^1 . **b**, Graphene dispersion-cones around one K -point of the graphene Brillouin zone. Due to SOI the spin-up (blue) and spin-down (red) Dirac cones are split in both the vertical (E) and k_{\perp} -direction. The cut shows the resulting CNT band structure also shown in the upper inset in **a**.